# Perrhenate Incorporation into Binary Mixed Sodalites: The Role of Anion Size and Implications for Technetium-99 Sequestration

**Johnbull O. Dickson*[1], James B. Harsh[1], Markus Flury[1], Wayne W. Lukens[2], and Eric M. Pierce[3],**

[1]Department of Crops and Soil Sciences, Washington State University, P. O. Box 646420, Pullman, WA 99164, USA

[2]Chemical Sciences Division, Lawrence Berkeley National Laboratory, Berkeley, CA 94720

[3]Environmental Sciences Division, Oak Ridge National Laboratory, P. O. Box 2008, Oak Ridge, TN 37831.

*Corresponding Author: J.dickson@wsu.edu

**ABSTRACT:**

Perrhenate ($ReO_4^-$), as a $TcO_4^-$ analogue was incorporated into mixed-anion sodalites from binary solutions containing $ReO_4^-$ and a competing anion $X^{n-}$ ($Cl^-$, $CO_3^{2-}$, $SO_4^{2-}$, $MnO_4^-$, or $WO_4^{2-}$). Our objective was to determine the extent of solid solutions formation and the dependence of competing ions selectivity on ion size. Using equivalent aqueous concentrations of the anions ($ReO_4^-$/ $X^{n-}$ molar ratio = 1:1), mixed-anion sodalites were hydrothermally synthesized from zeolite and NaOH at 90°C for 96 hours. The resulting solids were characterized by bulk chemical analysis, X-ray diffraction, scanning electron microscopy, and X-ray absorption near edge structure (XANES) spectroscopy to determine the crystal structure, chemical composition, and morphology, and to confirm the rhenium (Re) oxidation state. Rhenium in the solid phase occurred predominately as $Re(VII)O_4^-$ in the sodalite, which has a primitive cubic pattern in the space group $P\bar{4}3n$. The refined unit-cell parameters of the mixed sodalites ranged from 8.88 to 9.15 Å and showed a linear

dependence on the size and mole fraction of the incorporated anion(s). The $ReO_4^-$ selectivity, represented by its distribution coefficient, increased in the following order: $Cl^-<NO_3^-<MnO_4^-$ and $CO_3^{2-}<SO_4^{2-}<WO_4^{2-}$ for the monovalent and divalent anions respectively. The relationship between $ReO_4^-$ distribution coefficient and competing anion size was nonlinear. When the difference in ionic radius (DIR) between $ReO_4^-$ and $X^{n-}$ (n = 1 or 2) was greater than ~12% $ReO_4^-$ incorporation was insignificant. The results imply that anion size is the major factor that determines sodalite anion compositions and that $ReO_4^-$ is likely to serve as a suitable analogue for $TcO_4^-$ where Tc(VII) is the stable oxidation state.

## ■ INTRODUCTION

The application of versatile porous framework materials (feldspathoids) as a selective medium for sequestration of key anionic radionuclides is of paramount importance to the nuclear waste industry. Furthermore, advanced knowledge of factors governing anion selectivity in feldspathoids is critical for their potential application in anion-sequestration processes[1]. The safe disposal of nuclear waste generated by the nuclear fuel cycle remains one of the most challenging, and potentially costly, environmental endeavours of the 21st century [2]. In generation of 20% of the U.S. electricity by nuclear power plants and the rising demand for nuclear power arises a host of waste issues and the technical challenge of immobilizing high-level nuclear wastes (HLW) for temporary storage or disposal in geologic repositories [3]. While glass (borosilicate) waste forms have been employed to immobilize high level nuclear waste (HLW) from nuclear weapons programs and spent nuclear fuel (SNF) from commercial nuclear power plants, ceramic (zirconolite, apatite, Synroc, pyrochlore) and glass ceramic (titanite, celsian, zirconolite silicotitantates, and apatitic) waste forms have been proposed for immobilization of defense HLW and spent nuclear fuel [3]. Vitrification processes are currently employed to treat commercial HLW at West Valley site (New York) and defense HLW at DOE Savannah River site (Aiken, South Carolina); while at the DOE Hanford site (Washington), construction of a vitrification plant is underway to immobilize defense HLW [3].

It has been shown that percolating pore water reacts with glass waste forms to form more stable secondary phases, including zeolite (analcime), smectite (Na-beidellite), and feldspathoids [4, 5]. As products of chemical weathering, these secondary mineral phases can potentially retain radionuclides released from corroding vitreous waste forms in their frameworks, thereby controlling the fate and transport of key radionuclides in the environment. Detailed understanding of anion selectivity in porous framework materials (feldspathoids) is critical to understanding the long term

fate of anionic radionuclides in the environment.

Feldspathoids such as cancrinite and sodalite have crystalline microporous framework structures. They can be represented by the general formula: $A_8[TO_4]_6X_2$ where T is Al and/or Si and, A and X are monovalent or divalent cations and anions, respectively [6]. Sodalite consists of corner sharing $SiO_4$ and $AlO_4$ tetrahedra constructed into four and six-membered rings that form the cuboctahedral cages referred to as sodalite β-cages. The sodalite framework can be considered as a space-filling arrangement of the sodalite β-cages directly linked via the six-membered rings to form the semi-condensed sodalite structure. In the center of the cage is an anion that is tetrahedrally coordinated to four cations, forming $A_4X$ clusters [7].

Feldspathoids with guest ions in their structures have been widely studied [8]. Most studies have been devoted to mixed cation substitutions in sodalite frameworks [9, 10] and to single anion sodalites [11, 12]. Multiple anion substitution in sodalite is less well characterized. Understanding sodalite selectivity for anionic species of varying sizes is important for elucidating anion substitution in mixed sodalite with more complex structures, especially those sodalites containing key anionic radionuclides ($^{125}I$, $^{99}Tc$, $^{75}Se$).

While it seems likely that $TcO_4^-$ would be trapped by feldspathoid phases during glass corrosion, previous studies of waste glass weathering show that $^{99}Tc$ is released congruently with boron during. (ref: Bibler, N.E.; Jurgensen, A.R. "Leaching $^{99}Tc$ form SRP Glass in Simulated Tuff and Salt Groundwaters" Mat. Res. Soc. Symp. Proc. **1988**, *112*, 585-593.) This contradiction illustrates that exist significant gaps in our current understanding of the role of sodalite selectivity as a driving force for controlling the fate and transport of key radionuclides in the subsurface. Previous work with $NO_3^-/ReO_4^-$-sodalites suggested that selectivity is anion size-dependent [13]. Therefore, we investigated the competitive incorporation of $ReO_4^-$ into mixed anion-bearing sodalite in the presence of these competing anions ($X^{n-}$) ranging in size and charge: $Cl^-$, $CO_3^{2-}$, $SO_4^{2-}$, $MnO_4^-$, and

$WO_4^{2-}$. We used Re as a nonradioactive analogue for Tc. Under aerobic (oxic) conditions both elements are stable as oxyanions ($ReO_4^-$ and $TcO_4^-$), which have similar metal oxygen bond lengths (Tc–O = 1.702 Å and Re–O = 1.719 Å) and ionic radii ($TcO_4^-$ = 2.52 Å and $ReO_4^-$ = 2.60 Å)[14-16]

This study highlights the dependence of selectivity on ion size and charge. Additionally the variation of the sodalite structural parameter as a function of composition (anion mixing) will shed light on the extent of anion incorporation into mixed sodalites formed in environmentally relevant conditions such as subsurface and engineered wastes, vitrification products, and materials formed by chemical weathering.

## ■ MATERIALS AND METHODS

**Hydrothermal Mineral Synthesis.** Mixed-anion sodalites with $ReO_4^-$ and one other anion ($X^{n-}$) were hydrothermally synthesized based on modification of a method previously described by Liu and Navrotsky [17]: Sodium hydroxide (Alfa Aesar) was mixed with zeolite 4A ($Na_{12}Al_{12}Si_{12}O_{48}$ $xH_2O$, W.R Grace & Co.) and sodium salts of the appropriate anions. The zeolite supplied a 1:1 molar ratio of Si/Al. The mixed sodalites were synthesized in a 60-mL Teflon digestion bomb filled with 20 mL of de-ionized water, 1 g of NaOH pellets (1.25 *M* NaOH) and 0.5 g of zeolite. To these basic solutions, 0.88 *M* of $NaReO_4$ was added and 0.88 *M* of $Cl^-$, $CO_3^{2-}$, $SO_4^{2-}$, $MnO_4^-$, or $WO_4^{2-}$was added as the competing anion. All chemical reagents were used as received. The bombs were capped, and aged for 96 hours in a 90°C oven. After decanting the basic supernatant solutions the solid precipitates were washed three times with deionized water ($0.054 \times 10^{-3}$ $dSm^{-1}$). The solids were dialyzed in deionized water until the electrolytic conductivity was ≤0.01 $dSm^{-1}$, dried for 24 hours, and weighed. Solid yield after dialysis ranged from 0.5 to 0.6 g.

**Powder X-ray Diffraction**. X-ray diffraction data were obtained with a Panalytical Xpert Pro diffractometer (XRD) scanning at 1.5°/min over 5 – 90° 2θ. We used $CoK_\alpha$ radiation (λ =

1.789010 Å) and an X'Celerator silicon strip detector equipped with an Fe filter. Scans used ¼° fixed divergence slits and ½° anti-scatter slit. "Jade" and/or High Score Plus software, and the ICDD database were used for mineral identification. Rietveld refinements of the XRD data were performed in High Score Plus and/or GSAS with EXPGUI interface [18] using the reported structures of the following phases: $Na_8(AlSiO_4)_6(NO_2)_2$ [19], $Na_8(AlSiO_4)_6(ReO_4)_2$ [20], and $Na_6Ca_{1.5}(AlSiO_4)_6(CO_3)_{1.5}(H_2O)_{1.75}$ [21]. The following parameters were allowed to vary: the background (8 parameters), unit cell, Na position, Re/anion occupancy, peak shape (5 parameters: U, V, W, and two peak shape parameters), overall thermal parameter (B), and preferred orientation.

**X-ray Absorption Near Edge Structure (XANES) Spectroscopy.**

Powdered sodalite samples were mixed with boron nitride and mounted on an aluminum holder with Kapton windows. The XANES spectra were obtained at the Stanford Synchrotron Radiation Lightsource (SSRL) using the 11-2 beamline equipped with a Si (220) double crystal monochromator ($\phi$ = 90 crystals) detuned 50% to reduce the harmonic content of the beam. The spectra from 0.2 keV below to 10 keV above the Re $L_2$-edge (11.959 keV) were collected either in transmission mode using nitrogen-filled ion chambers or fluorescence mode using a 100-element Ge detector and corrected for detector dead time. We converted raw data to spectra and normalized with SixPack and Artemis [22]. Normalized XANES spectra were fit using standard spectra in the locally written program 'fites', which utilizes a non-linear least squares fitting data. Two reference spectra, $ReO_2$, and pure $ReO_4$-sodalite, were used for data fitting. The sample XANES spectra were allowed to vary in energy during fitting and the spectral resolution is 7 eV based on the width of the white line at the Re $L_2$-edge.

**Electron Microscopy.** Scanning electron micrographs (SEM) were obtained with platinum-palladium sputter-coated powder samples. The coated powder samples were examined under field emission scanning electron microscope (FESEM) (FEI Quanta 200F, FEI Co., Hillsboro, OR).

**Chemical Analysis.** The powder samples digested in 3% nitric acid were analyzed for Na concentration by atomic emission and/or absorption spectrophotometry (Varian 220 Flame Atomic Absorption Spectrometer, Varian Ltd., Mulgrave, Australia). The Si, Al, Mn, W, and Re concentration in the solids were determined by inductively coupled plasma-mass spectrometer (Agilent 7700 ICP-MS, Santa Clara, CA) and concentrations of Cl and, S by ion chromatography (HPLC-10Ai, Shimadzu Inc., Canby, OR). Total carbon concentration was determined by dry combustion from TruSpec C/N analyzer (Leco Corporation, St. Joseph, MI) equipped with a high temperature combustion method and infrared detection technique.

## ■ RESULTS

**Synthesis Product Morphology:** The SEM images of the mixed-anion sodalites are shown in Figure 1. The mixed-anion sodalites formed in the presence of $Cl^-$, $CO_3^{2-}$, $MnO_4^-$ and $WO_4^{2-}$ had hexagonal euhedral crystals (Figure 1A -B, D-E). The observed morphology differs from the lepispheric morphology reported by Deng et al, (2006) for precipitates formed from simultaneous additions of two or more anions ($Cl^-$, $NO_2^-$, $NO_3^-$, $CO_3^{2-}$, $SO_4^{2-}$, $PO_4^{3-}$) to starting solutions of Na hydroxide, aluminate, and silicate. In contrast, our experiments used zeolite as Al and Si source. The crystalline solids formed in the presence of $SO_4^{2-}$ anions were dominated by lepispheric and lenticular-shaped crystal structures, comprised of inter-grown thin disks or blades (Figure 1C). The observed $ReO_4^-/SO_4^-$-sodalite morphology was similar to those reported by Deng et al, (2006) for precipitates formed in binary or multi-anion solutions. Particle size measurements data for the mixed-anion sodalites are presented in Table 1. The particle sizes were consistent with those reported by Missimer et al.[23] for similar phases. Differences among the mixed-anion sodalite phases are due either to the degree of crystal growth or the amount of agglomeration.

**Composition Analysis.** The chemical composition of the synthesis products is shown in Table 2. The mixed-anion sodalites contained from 0.02 – 1.49 mole $ReO_4^-$ and 0.04 – 2.10 mole of

$X^{n-}$ per formula unit. The sodalites synthesized in the presence of $ReO_4^-$ and $Cl^-$, $CO_3^{2-}$, or $SO_4^{2-}$ incorporated negligible amounts of $ReO_4^-$. In contrast, the sodalite cages exhibited strong preference for $ReO_4^-$ over $WO_4^{2-}$ with ~95% $ReO_4^-$ occupancy of available sites. Further evidence of $ReO_4^-$ incorporation into sodalite is shown in the energy-dispersive X-ray spectroscopy (EDS) patterns (Figure 2). Perrhenate was best incorporated into the $ReO_4^-/MnO_4^-$ and $ReO_4^-/WO_4^{2-}$-sodalites whereas insignificant incorporation into the $ReO_4^-/Cl^-$, $ReO_4^-/SO_4^{2-}$ and $ReO_4^-/CO_3^{2-}$-sodalites occurred.

**Mineral Structure.** The calculated XRD patterns obtained from the Rietveld refinements of the mixed-anion sodalites are displayed in Figure 3. The refined lattice parameter, (*a*) and index of agreement ($\chi^2$) for the mixed-anion sodalites are shown in Table 3. The space group $P\bar{4}3n$ was adopted for the mixed-anion sodalite with *a* ranging from 8.8885(2) to 9.1527(1) Å. The Rietveld refinements indicate small amounts of cancrinite were formed along with the dominant sodalite phase(s).

**Rhenium Oxidation State.** The spectra fitting were performed as described by Lukens et al. [24, 25]. The Re $L_2$ edge XANES data were fit using only the spectra of $ReO_2$(s) and $ReO_4^-$-sodalite. The spectrum $ReO_4^-/MnO_4^-$-sodalite is presented in Figure 6. In the mixed-anion sodalites, the spectrum of $ReO_4^-$-sodalite contributes significantly (≥92%) to the fit and only in the presence of $Cl^-$ does the spectrum of $ReO_2$ contribute significantly to greater than 2σ of the fit (Table 4). Thus, the $ReO_4^-$ species is considered the dominant rhenium species in these solid phases.

## ■ DISCUSSION

**Incorporation of $ReO_4^-$ in the Presence of Competing Anion ($X^{n-}$).** Using an equal concentration of $ReO_4^-$ and $X^{n-}$ in the starting solutions, we synthesized five mixed-anion sodalites and tested the hypotheses that ionic sizes and mole fraction determine the lattice parameter and that

ion size and charge drive the selectivity between the two anions.

As the ionic radius increases in the following series: $Cl^- < CO_3^{2-} < SO_4^{2-} << MnO_4^- < WO_4^{2-}$ the selectivity of $ReO_4^-$ for the mixed sodalite linearly increased (Figure 4), consistent with the linear expansion of the cages from the $ReO_4^-/Cl^-$-sodalite to the $ReO_4^-/WO_4^-$-sodalites. Vegard's Rule [$a_{AB} = a_A(M_A) + (M_{1-A})a_B$] predicts a linear relationship between the crystal lattice parameter of solid solutions ($a_{AB}$) and a weighted average size based on concentrations ($M_A$, $M_{1-A}$) and radii of the constituent elements A and B. The rule is expected to hold for well-mixed solid solutions; however, substantial differences in anion size may lead to phase separation and differences in charge to incomplete cage filling. The larger the difference in size between $ReO_4^-$ and the competing anion, the more likely are the deviations from their random distribution in the sodalite lattice leading to noncompliance with Vegard's Rule. Similarly, anions of greater charge will not occupy all cages. Because negligible amounts of $ReO_4^-$ were incorporated into the $Cl^-$, $CO_3^{2-}$, and $SO_4^{2-}$-sodalites, the observed linear fit due to the size of the three ions does not imply phase separation. Moreover the mixed sodalites that contained significant amounts of each anion also fit the line generated by Vegard's Rule, suggesting that the $ReO_4$-sodalites containing $MnO_4^-$ or $WO_4^{2-}$ are well-mixed solid solutions. Only $CO_3^{2-}$ deviates significantly from the line, which is likely due to the fact that only half the cages can be occupied to maintain charge balance.

The inability to form mixed sodalites containing significant $ReO_4^-$ in the presence of $Cl^-$, $CO_3^{2-}$, and $SO_4^{2-}$ is due the large size difference between $ReO_4^-$ and the competing anions. According to Hume-Rothery Rules, the following conditions favor solid solution formation: similarity in the resulting crystal structure and ion valency, electronegativity and size. Sodalite cages can host anions of varying size due to cooperative tilting and deformation of the frameworks up to a point. Trill et al. (2003) state that the difference in anion size may not exceed 15%, because of excessive strain on the sodalite framework [26]. This behaviour is illustrated in our system in Figure

5 where anion selectivity is plotted against the difference in ionic radii (DIR) of solvent A ($r_A$) and solute B ($r_B$) in where:

$$\text{DIR}\ (\%) = \left(\frac{r_A - r_B}{r_B}\right) \times 100$$

As DIR increases from 2.7% in the $ReO_4$/$WO_4$-sodalite to 51.2% in the $ReO_4$/Cl-sodalite, the $ReO_4^-$ distribution coefficient exponentially declines from 3.73 to 0.02. When the difference in ionic radii (DIR) between $ReO_4^-$ and the competing anion exceeds 15%, the concomitant inclusion of both anions would sufficiently distort the mixed-anion sodalite cages, resulting in the exclusion of the larger anion from the cages. This is manifested in the preferential formation of mostly $Cl^-$, $CO_3^{2-}$ and $SO_4^{2-}$-sodalites containing minor amounts of enclathrated $ReO_4^-$. Although the DIR for $ReO_4^-$/$SO_4^{2-}$ (13%) and $ReO_4^-$/$WO_4^{2-}$-sodalites (2.7%) should favor the formation of mixed sodalite solid solutions, the distribution coefficient shows a clear preference for $SO_4^{2-}$ and $ReO_4^-$ respectively. In the case of $SO_4^{2-}$, DIR is close to 15%, indicating that this difference is still large enough to strongly favor the smaller anion. For $WO_4^{2-}$, the difference in charge and inability to fill all cages with either $ReO_4^-$ or $WO_4^{2-}$ may explain $ReO_4^-$ preference.

**Environmental Implications for $^{99}$Tc Immobilization.**

In this study, five mixed-anion sodalites containing extra-framework species were synthesized and characterized. The selectivity for intra-lattice anions of the products was highly dependent on the size and, to a lesser extent, the charge of the competing anion. The results of our study suggest that similarity in ionic radius (DIR of ≤15%) and charge (ionic potential) promote the competitive incorporation of $ReO_4^-$ into the mixed-anion sodalite (Figure 5 and Table 5). Selectivity

of $ReO_4^-$ for the mixed-anion sodalite was found to increase in the series as follows: $Cl^- < CO_3^{2-} < NO_3^- < SO_4^{2-} << MnO_4^- < WO_4^{2-}$

The findings in this study have implications for the fate and transport of $^{99}TcO_4^-$ in subsurface sediments assuming that its chemical behavior can be well approximated by $ReO_4^-$. Firstly, the formation of a $ReO_4^-/MnO_4^-$-sodalite solid solution implies that $ReO_4^-$ is a suitable analogue for $TcO_4^-$. Like $TcO_4^-$, $MnO_4^-$ shares a similar size, ionic potential, and electronegativity with $ReO_4^-$ (Table 5). The solid solution is consistent with Vegard's Rule, and the distribution coefficient for $ReO_4^-$ was unity, implying nearly equal selectivity for $MnO_4^-$- and $ReO_4^-$ during the formation of sodalite. The same is likely to be true for $TcO_4$-sodalite.

Our results also suggest that while neoformed feldspathoid minerals, such as sodalite, can incorporate $^{99}Tc$ as $TcO_4^-$, smaller competing anions will be preferred. Unfortunately, in many cases where environmental conditions are conducive for feldspathoid formation, the waste solutions may also contain high concentrations of such competing anions. In the case of waste glass corrosion, the primary competing anions are hydroxide and carbonate. Consequently, any sodalite formed during glass corrosion will preferentially incorporate these small anions, allowing $TcO_4^-$ to leach from the glass as previously observed.

~~One limitation of our results is that sodalite synthesis occurred in a closed system. In open, free-flowing systems, the smaller anions may become depleted leaving $TcO_4^-$ to be incorporated later in the waste stream~~ (my understanding is that this is only true for hydroxide as was stated in the previous paper.) Our experiments were designed specifically to form sodalite phase because of the ability of its cages to sequester large ions such as $TcO_4^-$. In other systems, neoformed mineral phases could include zeolite, nosean, and nepheline. It has been reported that $NO_3^-$ will sequester into cancrinite and $SO_4^{2-}$ into nosean; whereas $Cl^-$ and $ReO_4^-$ will be incorporated into mixed

sodalite [27]. Thus, at the comparatively low concentrations of $TcO_4^-$ ($10^{-6}$ to $10^{-4}$ M) expected in most nuclear waste streams, $TcO_4^-$ could intercalate into the mixed-anion sodalite phases after other competing anions have been selectively sequestered into their respective neoformed mineral phases. Further work is needed in open systems, with a greater range of conditions, and at realistic $^{99}Tc$ concentrations to mimic waste-impacted subsurface sediments, managed waste streams, and vitrification systems to determine if mixed-anion sodalites may be relevant sequestering phase(s).

## ■ ACKNOWLEDGEMENT

This material is based upon work supported by the U.S. Department of Energy (DOE), Office of Science, Biological and Environmental Research Program (SBER), under contract No. DE-PS02-09ER65075. This work was funded by the U.S. Department of Energy, Office of Science, Biological and Environmental Research, Subsurface Biogeochemical Research Program. ORNL is operated by UT-Battelle, LLC for DOE under Contract No. DE-AC05-00OR22725. Portions of this work were supported by DOE, Office of Science, Basic Energy Sciences, Chemical Sciences, Biosciences, and Geosciences Division, Heavy Element Chemistry Program and were performed at Lawrence Berkeley National Laboratory under Contract No. DE-AC02-05CH11231. Portions of this work were performed at the Stanford Synchrotron Radiation Lightsource (SSRL), which is a DOE Office of science user facility operated by Stanford University. We are also indebted to the staff at the Franceschi Microscopy and Imaging Center at Washington State University for access to and assistance with the use of their SEM facilities.

## ■ REFERENCES


[1] R. Custelcean, B.A. Moyer, Anion separation with metal-organic frameworks, Eur J Inorg Chem, (2007) 1321-1340.

[2] R.C. Ewing, Nuclear waste forms for actinides, Proceedings of the National Academy of Sciences of the United States of America, 96 (1999) 3432-3439.

[3] W.J. Weber, A. Navrotsky, S. Stefanovsky, E.R. Vance, E. Vernaz, Materials Science of High-Level Nuclear Waste Immobilization, MRS Bull, 34 (2009) 46-53.

[4] S.V. Mattigod, J. Serne, B.P. McGrail, V.L. LeGore, Radionuclide Incorporation in Secondary Crystalline Minerals from Chemical Weathering of Waste Glasses. MRS Proceedings, 713, JJ5.1 in: B.P. McGrail, G.A. Cragnolino (Eds.) Scientific basis for nuclear waste management XXV, Material Research Society, Warrendale PA, Boston, MA, 2002.

[5] Y. Inagaki, K. Idemitsu, T. Arima, T. Maeda, H. Ogawa, F. Itonaga, Alteration-phase formation and associated cesium release during alteration of R7T7 waste glass, in: B.P. McGrail, G.A. Cragnolino (Eds.) Scientific basis for nuclear waste management XXV, Material Research Society, Warrendale PA, Boston, MA, 2002.

[6] D. Taylor, C.M.B. Henderson, A computer model for the cubic sodalite structure, Phys Chem Miner, 2 (1978) 325-336.

[7] H. Trill, Sodalite solid solution systems: Synthesis, topotactic transformations, and Investigation of framework-guest and guest-guest interactions, Universität Münster 2002, pp. 187.

[8] G.M. Johnson, P.J. Mead, M.T. Weller, Structural trends in the sodalite family, PCCP, 1 (1999) 3709-3714.

[9] M.E. Brenchley, M.T. Weller, Synthesis and structures of $M_8[AlSiO_4]_6(XO_4)_2$, M=Na, Li, K, X=Cl, Mn Sodalites, Zeolites, 14 (1994) 682-686.

[10] A. Stein, G.A. Ozin, G.D. Stucky, Class-B sodalites - nonstoichiometric silver, sodium halosodalites, JACS, 114 (1992) 8119-8129.

[11] M.T. Weller, G. Wong, Mixed halide sodalites, Eur J Solid State Inorg Chem, 26 (1989) 619-633.

[12] M.T. Weller, G. Wong, C.L. Adamson, S.M. Dodd, J.J.B. Roe, Intracage reactions in sodalites, Journal of the Chemical Society-Dalton Transactions, (1990) 593-597.

[13] J.O. Dickson, J.B. Harsh, M. Flury, W.W. Lukens, E.M. Pierce, Sequestration of perrhenate in competition with nitrate by sodalite, Environ Sci Technol, Submitted (2014).
[14] Y. Marcus, Thermodynamics of solvation of ions. Part 5 - Gibbs free energy of hydration at 298.15-K Journal of the Chemical Society-Faraday Transactions, 87 (1991) 2995-2999.
[15] B.A. Moyer, P.V. Bonnesen, Physical Factors in Anion Separation. Supramolecular chemistry of anions, in: A. Bianchi, K. Bowman-James, E. Garcia-Espana (Eds.), Wiley-VCH, New York1979.
[16] J.P. Icenhower, N.P. Qafoku, J.M. Zachara, W.J. Martin, The biogeochemistry of Technetium: A review of the behavior of an artificial element in the natural environment, American Journal of Science, 310 (2010) 721-752.
[17] Q. Liu, A. Navrotsky, Synthesis of nitrate sodalite: An in situ scanning calorimetric study, Geochim Cosmochim Acta, 71 (2007) 2072-2078.
[18] B.H. Toby, EXPGUI, a graphical user interface for GSAS, J Appl Crystallogr, 34 (2001) 210-213.
[19] J.C. Buhl, J. Lons, Synthesis and crystal structure of nitrate enclathrated sodalite $Na_8(AlSiO_4)_6(NO_3)_2$, J Alloys Compd, 235 (1996) 41-47.
[20] S.V. Mattigod, B.P. McGrail, D.E. McCread, L.Q. Wang, K.E. Parker, J.S. Young, Synthesis and structure of perrhenate sodalite, Microporous Mesoporous Mater, 91 (2006) 139-144.
[21] K. Hackbarth, T.M. Gesing, M. Fechtelkord, F. Stief, J.C. Buhl, Synthesis and crystal structure of carbonate cancrinite $Na_8(AlSiO_4)_6CO_3 3.4H_2O$, grown under low-temperature hydrothermal conditions, Microporous Mesoporous Mater, 30 (1999) 347-358.
[22] B. Ravel, M. Newville, Athena, Artemis, Hephaestus: Data analysis for X-ray absorption spectroscopy using Ifeffit, Journal of Synchrotron Radiation, 12 (2005) 537-541.
[23] D.M. Missimer, R.L. Rutherford, Preparation and initial characterization of fluidized bed steam reforming pure-phase standards, Savannah River National Laboratory, Aiken, SC, 2013.
[24] W.W. Lukens, D.A. McKeown, A.C. Buechele, I.S. Muller, D.K. Shuh, I.L. Pegg, Dissimilar behavior of technetium and rhenium in borosilicate waste glass as determined by X-ray absorption spectroscopy, Chem Mater, 19 (2007) 559-566.
[25] W.W. Lukens, J.J. Bucher, D.K. Shuh, N.M. Edelstein, Evolution of technetium speciation in reducing grout, Environmental Science & Technology, 39 (2005) 8064-8070.
[26] H. Trill, H. Eckert, V.I. Srdanov, Mixed halide sodalite solid solution systems. Hydrothermal synthesis and structural characterization by solid state NMR, J Phys Chem B, 107 (2003) 8779-8788.
[27] E.M. Pierce, W.W. Lukens, J.P. Fitts, C.M. Jantzen, G. Tang, Experimental determination of the speciation, partitioning, and release of perrhenate as a chemical surrogate for pertechnetate from a sodalite-bearing multiphase ceramic waste form, Appl Geochem, 42 (2014) 47-59.

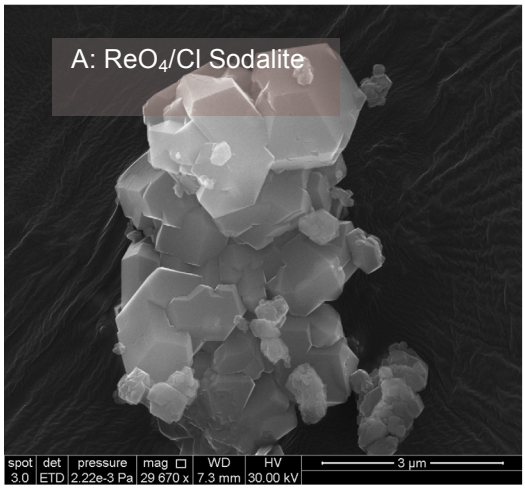
A: $ReO_4$/Cl Sodalite
spot det pressure mag WD HV
3.0 ETD 2.22e-3 Pa 29 670 x 7.3 mm 30.00 kV
3 µm

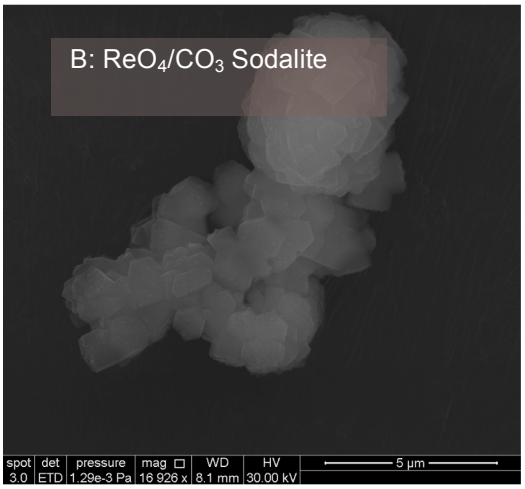
B: $ReO_4$/$CO_3$ Sodalite
spot det pressure mag WD HV
3.0 ETD 1.29e-3 Pa 16 926 x 8.1 mm 30.00 kV
5 µm

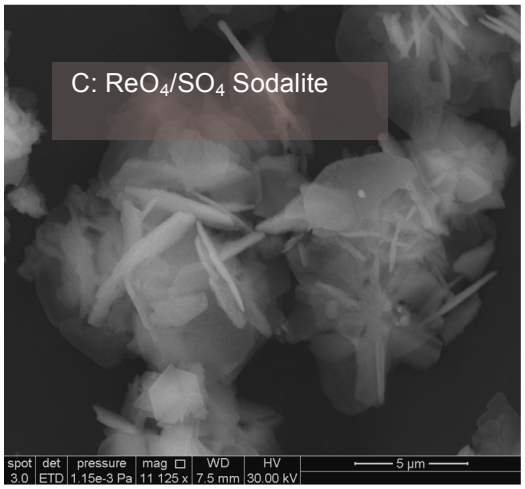
C: $ReO_4$/$SO_4$ Sodalite
spot det pressure mag WD HV
3.0 ETD 1.15e-3 Pa 11 125 x 7.5 mm 30.00 kV
5 µm

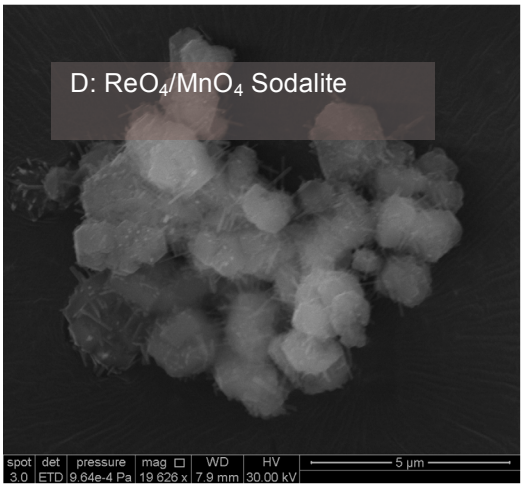
D: $ReO_4$/$MnO_4$ Sodalite
spot det pressure mag WD HV
3.0 ETD 9.64e-4 Pa 19 626 x 7.9 mm 30.00 kV
5 µm

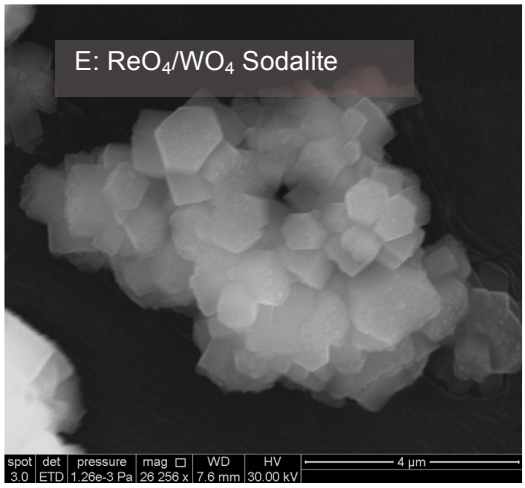
E: $ReO_4$/$WO_4$ Sodalite
spot det pressure mag WD HV
3.0 ETD 1.26e-3 Pa 26 256 x 7.6 mm 30.00 kV
4 µm

**Figure 1.** SEM micrographs of mixed-anion sodalite formed in 1:1 molar ratio of $ReO_4^-$/ $X^{n-}$ in solution

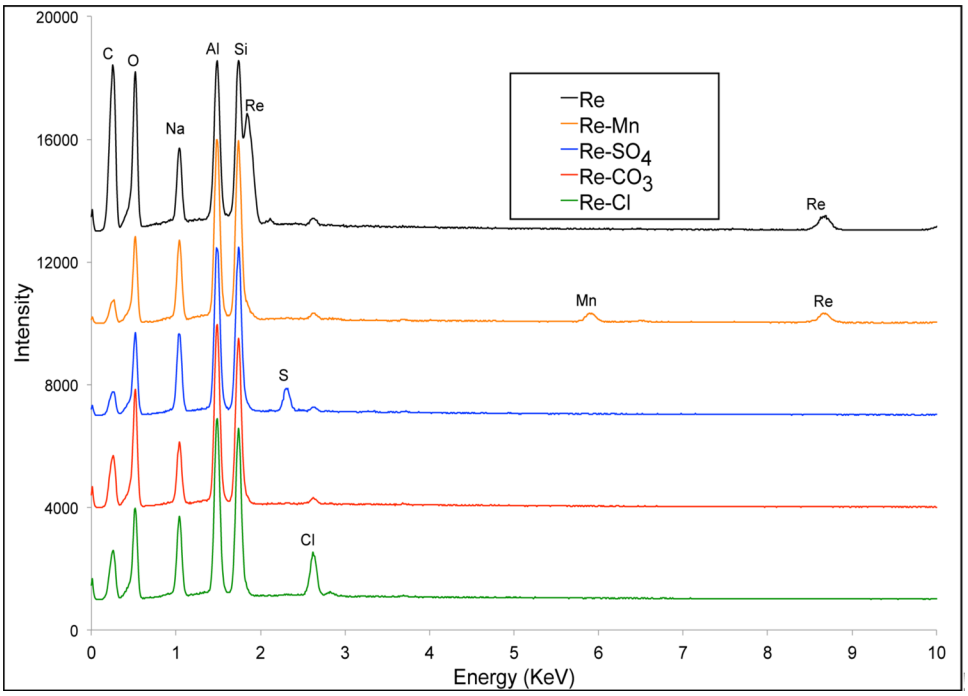


**Figure 2.** EDS spectra for select mixed anion sodalites: The additional Cl peaks in some of the samples are from the epoxy matrix used in preparing the samples for thin sections.

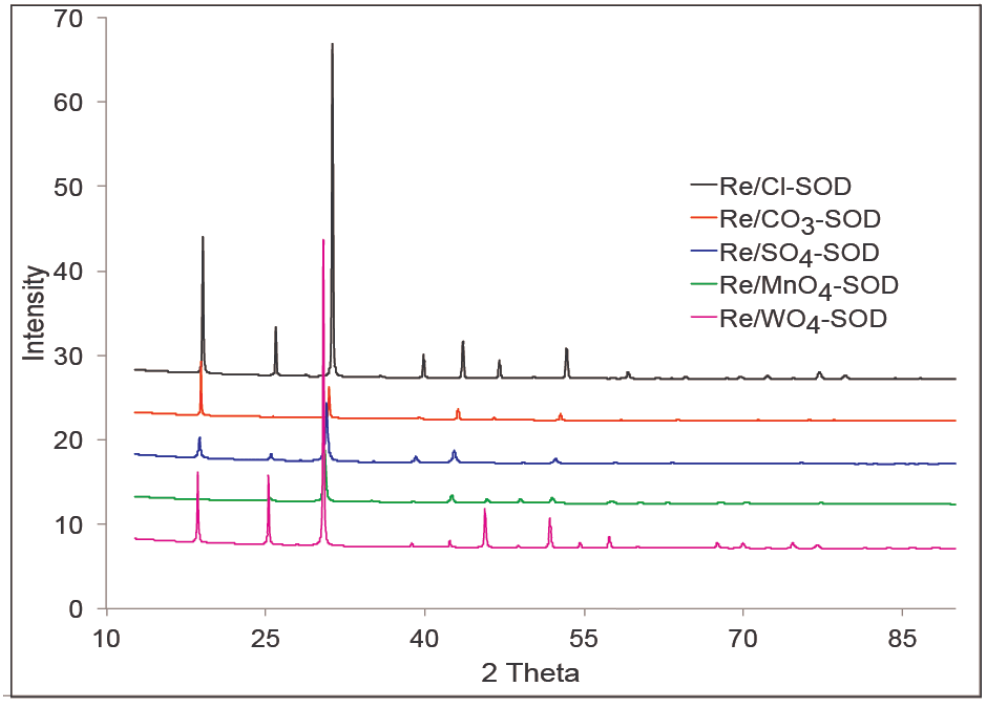

**Figure 3.** X-ray powder spectra for mixed-anion sodalites

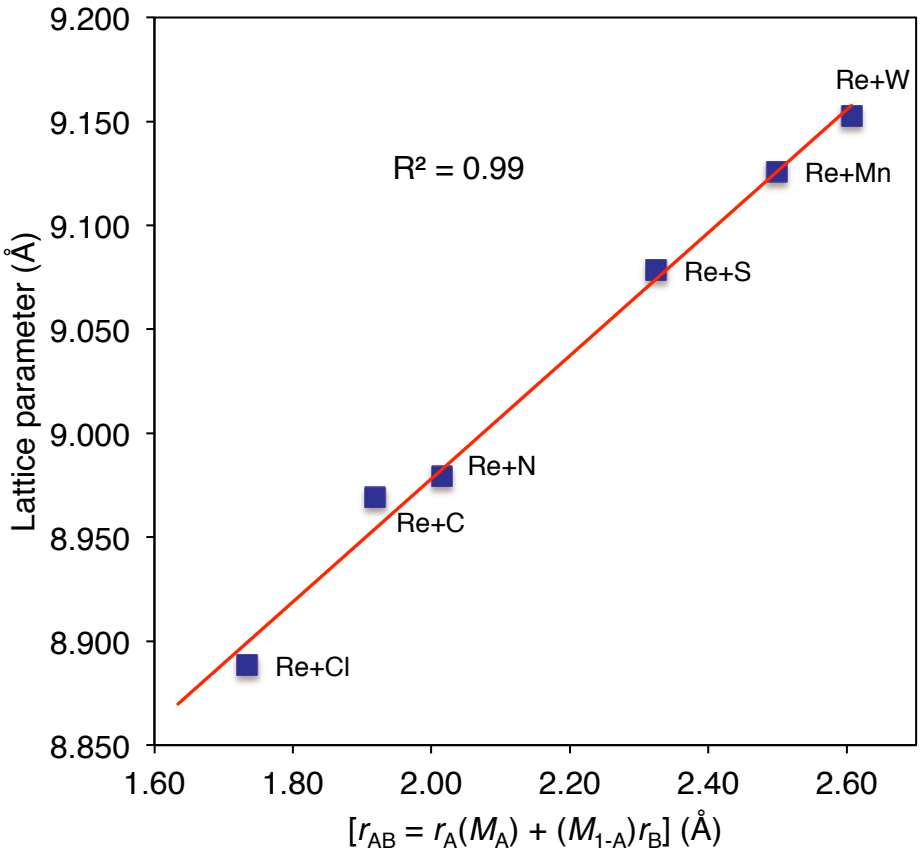


**Figure 4.** Graph showing the dependence of lattice parameter on [$r_{AB} = r_A(M_A) + (M_{1-A})r_B$]. Data points are from Rietveld refinement of XRD data, and the red line is based on Vegard's Rule.

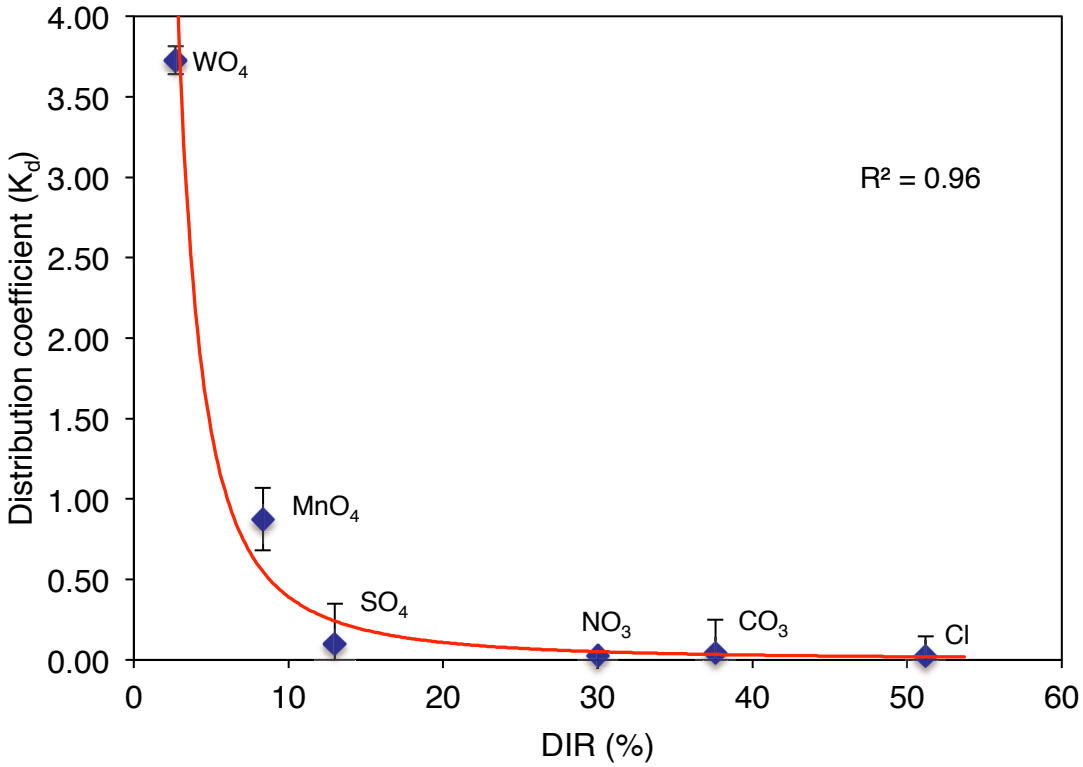


**Figure 5.** The distribution coefficient graph for $ReO_4^-$ sequestered in mixed-anion sodalite as a function of DIR; generally more than 90% of sodalite cages are filled with anions.

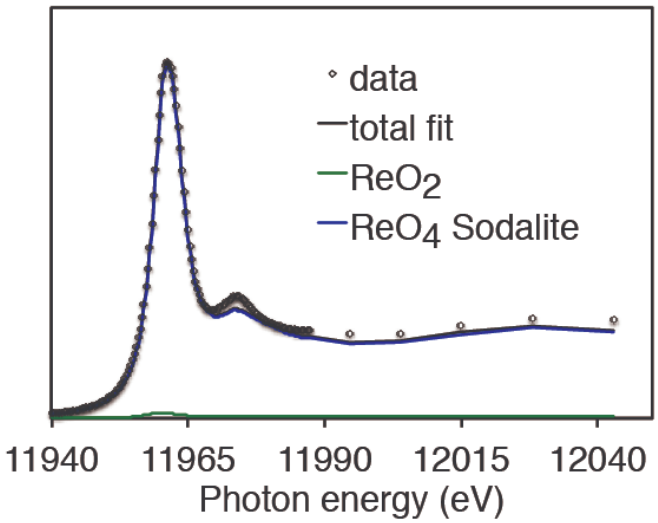


**Figure 6.** Re $L_2$-XANES spectral data for $ReO_4$/$MnO_4$-sodalite; data are represented by dots, and the fit is shown by the black line. Results indicate Re(VII) oxidation state.

**Table 1.** Particle Size Data (Mean Volume Distribution) for Mixed Anion Sodalites

| Percentile | Re/Cl-SOD Size (μm) | Re/$CO_3$-SOD Size (μm) | Re/$SO_4$-SOD Size (μm) | Re/$MnO_4$-SOD Size (μm) | Re/$WO_4$-SOD Size (μm) |
|---|---|---|---|---|---|
| 10 | 0.250 | 0.281 | 0.137 | 0.192 | 0.173 |
| 25 | 0.446 | 0.587 | 0.271 | 0.459 | 0.436 |
| 40 | 0.794 | 1.231 | 0.534 | 1.103 | 1.101 |
| 50 | 1.172 | 2.015 | 0.841 | 1.983 | 2.033 |
| 60 | 1.72 | 3.304 | 1.324 | 3.574 | 3.777 |
| 75 | 3.08 | 6.93 | 2.62 | 8.69 | 9.49 |
| 85 | 4.54 | 9.43 | 4.12 | 15.72 | 17.63 |
| 95 | 6.71 | 15.11 | 6.49 | 28.54 | 32.61 |

**Table 2.** Mixed Anion Sodalite Chemical Composition Data (mol/formula unit)

| **Structural Formula** | **Na** | **Al** | **Si** | **Re/X** | **$ReO_4$** | **X** |
|---|---|---|---|---|---|---|
| $Na_8[Al_6Si_6O_{24}](Cl_{(2.1)}ReO_{4(0.003)})$ | 7.96 ±0.16 | 6.00 ±0.05 | 6.06 ±0.11 | 0.00 | 0.003 ±0.001 | 2.14 ±0.07 |
| $Na_8[Al_6Si_6O_{24}](CO_{3(1.0)}ReO_{4(0.02)})$ | 8.00 ±0.30 | 6.01 ±0.11 | 6.00 ±0.10 | 0.02 | 0.021 ±0.005 | 1.01 ±0.10 |
| $Na_{7.6}[Al_6Si_6O_{24}](SO_{4(0.96)}ReO_{4(0.08)})$ | 7.61 ±0.07 | 6.02 ±0.07 | 6.08 ±0.07 | 0.08 | 0.080 ±0.002 | 0.958 ±0.12 |
| $Na_8[Al_6Si_{5.9}O_{24}](MnO_{4(1.1)}\ ReO_{4(0.97)})$ | 8.09 ±0.17 | 6.09 ±0.05 | 5.92 ±0.02 | 0.89 | 0.965 ±0.015 | 1.09 ±0.03 |
| $Na_{7.9}[Al_6Si_6O_{24}](WO_{4(0.05)}ReO_{4(1.9)})$ | 7.94 ±0.10 | 6.02 ±0.08 | 6.00 ±0.17 | 39.7 | 1.904 ±0.03 | 0.048 ±0.004 |

X – Anions ($Cl^-$, $CO_3^{2-}$, $SO_4^{2-}$, $MnO_4^-$, $WO_4^{2-}$)

**Table 3.** Refinement X-ray Data for Mixed-Anion Sodalite ($a_o$ – unit cell parameter, esd – estimated standard deviation, and $\chi^2$- index of agreement

| Sample Type | Structural Formula | $a_o$ (Å) | esd | $\chi^2$ |
|---|---|---|---|---|
| SOD-Re/Cl | $Na_8[Al_6Si_6O_{24}]( Cl_{(2.1)}ReO_{4(0.003)})$ | 8.8885 | ±0.0002 | 2.76 |
| SOD-Re/$CO_3$ | $Na_8[Al_6Si_6O_{24}]( CO_{3(1.0)}ReO_{4(0.02)})$ | 8.9691 | ±0.0002 | 8.07 |
| SOD-Re/$SO_4$ | $Na_{7.6}[Al_6Si_6O_{24}]( SO_{4(0.96)}ReO_{4(0.08)})$ | 9.0785 | ±0.0004 | 3.60 |
| SOD-Re/$MnO_4$ | $Na_8[Al_6Si_{5.9}O_{24}]( MnO_{4(1.1)} ReO_{4(0.97)})$ | 9.1258 | ±0.0005 | 1.32 |
| SOD-Re/$WO_4$ | $Na_{7.9}[Al_6Si_6O_{24}](WO_{4(0.05)}ReO_{4(1.9)})$ | 9.1527 | ±0.0002 | 6.05 |

**Table 4.** XANES Spectral Fitting Results for Mixed-anion Sodalites

| Sample | $ReO_2$ | p | $ReO_4$-sodalite | p |
|---|---|---|---|---|
| SOD-Re/Cl | 0.18(6) | 0.017 | 0.82(5) | <0.001 |
| SOD-Re/$CO_3$ | 0.08(5) | 0.168 | 0.92(4) | <0.001 |
| SOD-Re/$SO_4$ | 0.03(5) | 0.545 | 0.97(4) | <0.001 |
| SOD-Re/$MnO_4$ | 0.02(6) | 0.828 | 0.98(5) | <0.001 |
| SOD-Re/$WO_4$ | 0.00(2) | 1.000 | 1.00(1) | <0.001 |

a) The number in parentheses is the standard deviation in the same units as the preceding digit,
b) p is the usual p-value.

**Table 5:** Ionic Radii, Hydration Energy and Electronegativity Data for Studied Anions

| Anions (X) | r (nm) | DIR (%) | Ionic Potential (Z/r) | Hydration Energies ($kJmol^{-1}$) | $X_M$ ($kJmol^{-1}$) |
|---|---|---|---|---|---|
| $Cl^-$ | 0.172[d] | 51.2 | 0.58 | -340[a] | 800.10 |
| $CO_3^{2-}$ | 0.189[C] | 37.6 | 1.06 | -1315[a] | 604.24 |
| $SO_4^{2-}$ | 0.230[a] | 13.0 | 0.87 | -1080[a] | 599.80 |
| $NO_3^-$ | 0.200[a] | 30.0 | 0.50 | -300[a] | 704.65 |
| $MnO_4^-$ | 0.240[a] | 8.3 | 0.42 | -235[a] | 358.65 |
| $WO_4^{2-}$ | 0.267[b] | 2.7 | 0.75 | -702[e] | 424.30 |
| $ReO_4^-$ | 0.260[a] | 0.0 | 0.39 | -330[a] | 387.25 |
| $TcO_4^-$ | 0.252[d] | 3.2 | 0.40 | 251[d] | 377.50 |

Where r represents the ionic radius of the different anions: $Cl^-$, $CO_3^{2-}$, $SO_4^{2-}$, $MnO_4^-$, $WO_4^{2-}$, and $ReO_4^-$

$X_M$ (Mulliken electronegativity) = $(IE_v+EA_v)/2$; Where $IE_v$ refers to Ionization energy ($kJmol^{-1}$) and $EA_v$ is electron affinity ($kJmol^{-1}$)

*a: 1) Thermodynamics of solvation of Ions; Marcus et al. (1991)

*b: 2) Ionic radius in aqueous solution; Marcus et al. (1988)

*c: 3) Handbook of chemistry and physic; David et al. (2003)

*d: 4) Physical Factors in Anion Separation; Moyer et al. (1979)

*e: 5) Hydration and extraction of oxyanion; Abramov et al. (2001)

DIR: Differences in ionic radii